ACS Sustainable Chemistry & Engineering

pubs.acs.org/journal/ascecg

Research Article

Investigation of the Antiscaling Performance of Phosphonated Chitosan for Upstream Petroleum Industry Application

Mohamed F. Mady,* Safwat Abdel-Azeim, and Malcolm A. Kelland

Cite This: *ACS Sustainable Chem. Eng.* 2021, 9, 16494−16505

Read Online

ACCESS | Metrics & More | Article Recommendations | Supporting Information

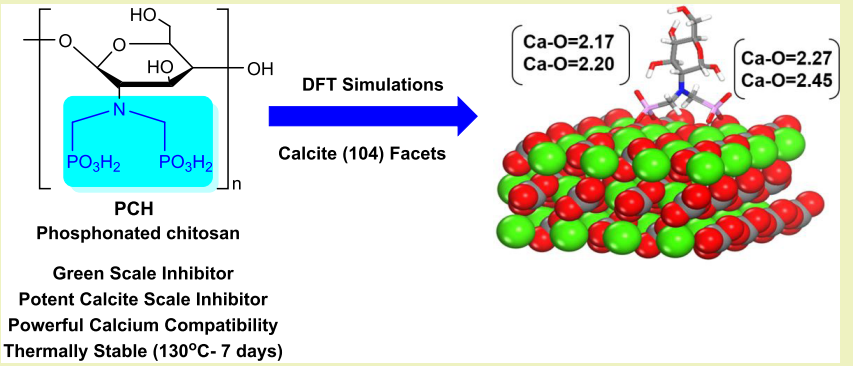

ABSTRACT: Scale deposition is one of the main water-based production problems in the upstream oil and gas industry. Few environmentally friendly scale inhibitors show good thermal stability as well as calcium compatibility. We report the synthesis of phosphonated chitosan (**PCH**) in a two-step route via a phosphonate ester. Chitosan is made from chitin, a natural polysaccharide. In dynamic tube blocking tests, **PCH** showed good performance as a calcium carbonate scale inhibitor, similar to some commercial nonpolymeric aminophosphonates. Performance was not lost even after thermal aging as a 5 wt % aqueous anaerobic solution for 1 week at 130 °C. The performance as a barite inhibitor was shown to be significantly worse. **PCH** showed excellent calcium compatibility from 100 to 10 000 ppm Ca^{2+} and 100 to 50 000 ppm **PCH** for 24 h at 80 °C. Density functional theory (DFT) and molecular dynamics (MD) simulations are employed to gain atomic insights into the interaction of **PCH** with the mineral surface as well as the polymer morphology. DFT predicts that **PCH** interacts as strongly as commercial scale inhibitors. MD simulations reveal a conformational contraction of **PCH** due to its internal hydrogen bonding network, which makes the inhibition mechanism complicated. Our simulation results bring new insights into the inhibition mechanism of polymeric inhibitors compared to small molecules. For example, a polymer with a well-defined structure such as carboxymethyl inulin (**CMI**) performs better than random folded polymers (**PCH**). The structural regularity maximizes the interaction sites of the mineral particles on the polymer surface. The compact morphology of **PCH** and the slow barite kinetics could be the main reason for the bad performance of **PCH** for barite scale inhibition.

KEYWORDS: *biopolymers, chitosan, phosphonates, scale inhibition, environmentally friendly scale inhibitors, calcium compatibility, oil and gas industry*

INTRODUCTION

The formation and deposition of inorganic salts in wells, flow lines, and processing equipment is one of the main flow assurance issues in the upstream petroleum industry.[1−4] These mineral salts are called scales and can be formed when the produced water is oversaturated beyond the thermodynamically stable limit. The commonest scales are calcium carbonate (calcite) and sulfate salts of calcium (gypsum), strontium (celestite), and barium (barite).

Prevention by treatment with chemical inhibitors is usually used to prevent scale deposition. Scale inhibitors are water-soluble chemicals that prevent or retard the nucleation and/or crystal growth of inorganic scales. Most scale inhibitors are either polymeric with many anionic groups (mostly carboxylate, sulfonate, or phosphonate) or can be smaller nonpolymeric molecules with one or more phosphonate groups, e.g., various aminophosphonates. Examples of classic oilfield scale inhibitors include phosphinopolycarboxylic acid (**PPCA**), acrylic acid/vinyl sulfonate copolymer (**AA/VS**), amino-

Received: October 5, 2021
Revised: November 12, 2021
Published: November 23, 2021

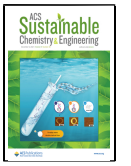

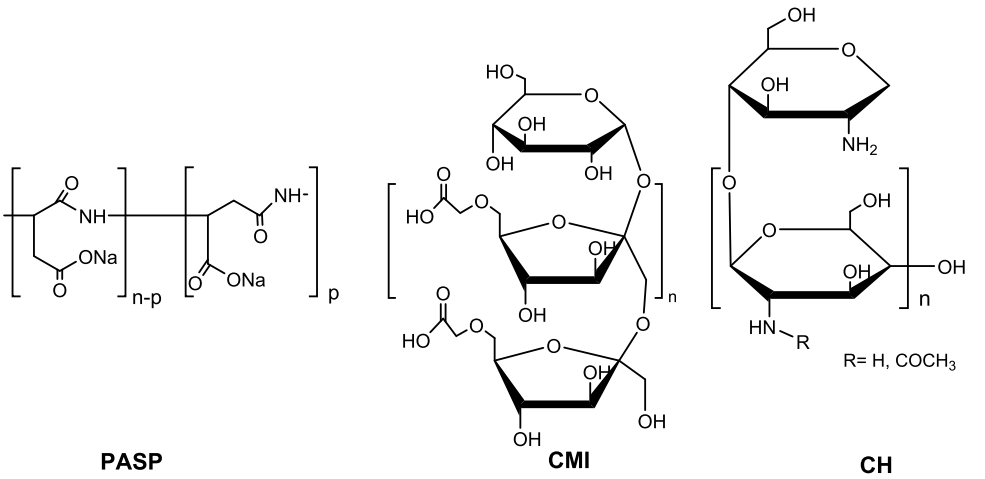

Figure 1. Chemical structures of polyaspartates (**PASP**), carboxymethyl inulin (**CMI**), and chitosan (**CH**).

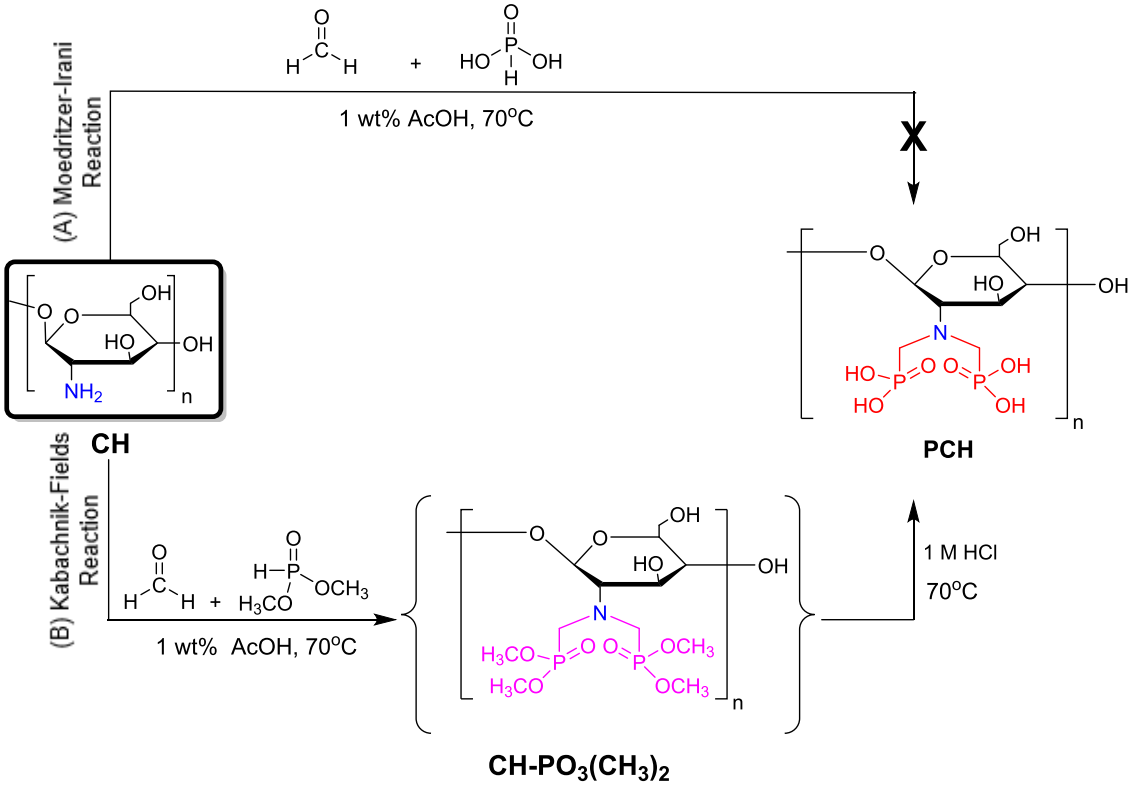

Figure 2. Schematic representation of phosphonated chitosan (**PCH**) via the Moedritzer−Irani reaction (route A) and the Kabachnik−Fields reaction (route B).

trimethylenephosphonate (**ATMP**), and diethylenetriamine-pentaphosphonate (**DTPMP**).[1−4]

Most scale inhibitors (SIs) have one or more drawbacks. For example, many of the best SIs are not very biodegradable, which limits their applications in areas with strict environmental regulations, such as offshore Norway. Several greener SIs have been developed, but they often have poor thermal stability, which means they are unsuitable for most downhole squeeze treatments unless the well temperature is low. Polymeric examples include classic polyaspartates (**PASP**) and polycarboxymethyl inulin (**CMI**, Figure 1).[5−9] Polyaspartate salts have also been used in squeeze treatments up to ca. 85 °C (185 °F), although an improved polyaspartate for squeezing up to 120 °C (248 °F) is reported to be available[1,10] Therefore, there is a particular need to develop more green SIs that have improved thermal stability.

Chitosan (**CH**) is the (almost fully) deacetylated version of chitin, a biodegradable biopolymer with a polysaccharide backbone and pendant amine groups (Figure 1). The precursor chitin is a homopolymer of β (1→ 4)-linked 2-acetamido-2-deoxy-β-D-glucose residues, which is hydrolyzed to form chitosan.[11,12] Chitosan is used in different applications, e.g., a flocculant and medical applications.[13] Recently, a water-soluble carboxymethyl chitosan (**CMCH**) has been reported as a green SI for oilfield calcite scale.[14] **CMCH** acts as a calcite scale inhibitor under synthetic brine medium, giving a minimum inhibitor concentration (MIC) of 170 ppm (1000 psi, T = 70 °C). Carboxymethyl quaternary ammonium

https://doi.org/10.1021/acssuschemeng.1c06786
ACS Sustainable Chem. Eng. 2021, 9, 16494−16505

oligochitosan and chitosan grafted with classic scale inhibitor vinyl monomers have also been studied as calcite scale inhibitors.[15,16]

However, the inclusion of phosphonate groups could be useful for improved performance. The most obvious way to include these groups is on the primary amine group of each saccharide ring. As the chitosan amine is primary, two phosphonate groups can be incorporated. As chitosan is a fairly high-molecular-weight polymer, phosphonates can be placed on a long chain length for better adsorption on scale surfaces or formation rock for squeeze treatments. It has been claimed that a general indicator of the inhibition strength of additives on the precipitation of barite scale is the number of phosphonate groups within the molecule.[17] However, some caution should be used, as other factors also determine the strength of inhibition, including structural matching with the crystal lattice, ease of removal of the hydration layer, degree of dissociation, complexation with ions in solution, and the ability to hydrogen bond. In addition, the greater the degree of dissociation of the inhibitor molecule, the better the inhibition (up to pH 8).

Demadis et al.[18−21] reported that phosphonated chitosan (**PCH**) can be used as an inhibitor of silicic acid polycondensation, but there appear to be no reports on calcite or barite inhibition.

Here, we report the barite scale inhibition of phosphonated chitosan (**PCH**) for the first time, as well as the first dynamic calcite scale inhibition study. We also report thermal stability and calcium compatibility studies to determine the viability of using **PCH** for downhole squeeze treatments.

EXPERIMENTAL SECTION

Materials and Instrumentation. Low-molecular-weight chitosan (mol. wt. = 50 000−190 000 Da) was purchased from Sigma-Aldrich and used as received. Other chemicals and reagents were acquired from Tokyo Chemical Industry Co., Ltd., VWR, and Sigma-Aldrich. All solvents were used as received without further purification. Distilled water (conductivity of 18 MΩ) was supplied from ELGA PURELAB Prima, Germany. Commercial samples of aminotrismethylenephosphonic acid (**ATMP**), diethylenetriaminepentamethylenephosphonic acid (**DTPMP**), and carboxymethyl inulin (**CMI**) were obtained from Italmatch Chemicals S.p.A., Italy.

^{1}H NMR, and ^{13}P NMR experiments were carried out at 25 °C on a 400 MHz Bruker nuclear magnetic resonance (NMR) spectrometer. A small amount of chitosan (20−50 mg) was dissolved in deuterium oxide (D_2O) with two drops of acetic acid. ^{1}H and ^{31}P NMR chemical shifts of phosphonated chitosan (**PCH**) were recorded in D_2O at 25 °C.

Synthesis of Phosphonated Chitosan as a Green Oilfield SI. *General Procedure for the Preparation of Phosphonated Chitosan (**PCH**) via the Moedritzer−Irani Reaction.* The attempted preparation of **PCH** was carried out as described previously in the literature by Heras et al. (Figure 2, route A).[22−24] Low-molecular-weight chitosan (2.5 g) was dissolved in an aqueous solution consisting of 1 wt % acetic acid (122.5 g) at 60 °C for 4 h. Phosphorous acid (H_3PO_3, 2.5 g) was dissolved in distilled water (5 mL) and then added slowly to the complete dissolution chitosan under vigorous stirring. The mixture solution was heated to 90 °C and then 4.5 mL of formaldehyde (HCHO) was added dropwise for ca. 1 h. The reaction solution was kept under continuous stirring for 80 h at 70 °C. The functionalized chitosan with phosphonate groups was monitored over the reaction period using ^{1}H and ^{13}P NMR spectroscopy. The polymer was precipitated by adding ethanol into the mixture solution, affording an off-white solid. The crude was concentrated by filtration and then analyzed by ^{1}H and ^{13}P NMR spectroscopy.

*General Procedure for the Preparation of Phopshonated Chitosan (**PCH**) via the Kabachnik−Fields Reaction.* The synthesis procedure of **PCH** was divided into two steps, as described previously in the literature by Illy et al. (Figure 2, route B).[25]

*(i). Synthesis of Phosphonated Diester Chitosan (**CH−PO$_3$(CH$_3$)$_2$**).* To a solution of low-molecular-weight chitosan (5.0 g, 30.4 mmol), acetic acid (1 wt %, 245.0 g) was added in a 500 mL round bottom flask. The reaction mixture was heated to 60 °C until the chitosan was completely dissolved in an acetic acid aqueous medium. Then, dimethyl phosphite $(CH_3O)_2PH$ (6.66 g, 60.4 mmol) and formaldehyde solution (7.08 g, 88.0 mmol) were added slowly with rapid stirring at 60 °C. The mixture solution was warmed to 70 °C and kept stirring for 96 h. The phosphonated diesters chitosan (**CH−PO$_3$(CH$_3$)$_2$**) intermediate was monitored by the ^{31}P NMR spectroscopy technique. The mixture solution was cooled, and 250 mL of isopropanol was added to the solution, affording an off-white solid (**CH−PO$_3$(CH$_3$)$_2$**). The solid was collected by filtration and dried under vacuum for 6 h. The final product was ready and used for the next step (hydrolysis stage) without further purification. ^{31}P NMR (D_2O, 162.00 MHz): δ 28.87.

*(ii). Synthesis of Phosphonated Chitosan (**PCH**).* To a stirred a solution of the obtained phosphonated diester chitosan (**CH−PO$_3$(CH$_3$)$_2$**), hydrochloric acid solution (1.0 mol L^{-1}, 70 mL) was added in a round bottom flask. The mixture solution was heated to 70 °C under vigorous stirring for 24 h. After completion of the hydrolysis reaction as monitored by ^{31}P NMR spectroscopy, the reaction mixture was cooled to room temperature, and then acetone was poured into the mixture to leave an off-white solid. The obtained solid was collected by filtration and then washed with acetone. Finally, the off-white solid was dried under reduced pressure for 6 h to afford a water-soluble phosphonated chitosan **PCH** (5.418 g), as shown in Figure 2. ^{31}P NMR (D_2O, 162.00 MHz): δ 10.31.

High-Pressure Dynamic Tube Blocking Test Methods. Dynamic tube blocking tests to determine relative scale inhibitor performance were carried out on an automated rig (built by Scaled Solutions Ltd., Scotland) at 100 °C and 80 bars using a 1 mm internal diameter 316 steel test coil (Figure 3). The inhibition of both calcite and barite scales was investigated. Details of the test procedure have been given previously.[26−33]

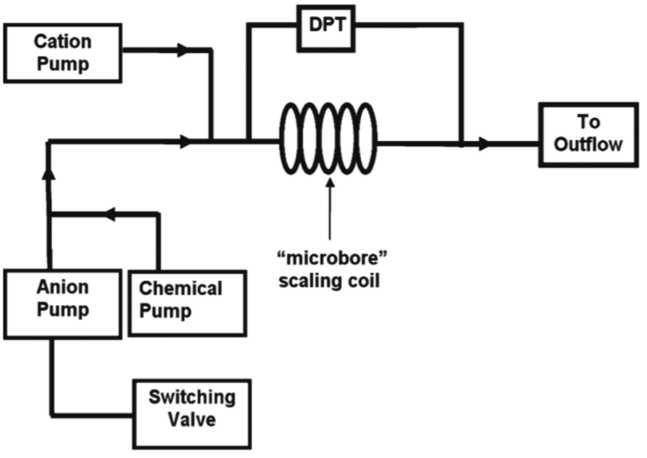

Figure 3. Schematic diagram of the dynamic tube blocking rig.

The highest test scale inhibitor concentration was 100 ppm, continued with descending concentrations (50, 20, 10, 5, 2, and 1 ppm) according to the SI performance. The concentration at which rapid tube blocking occurs was taken as the fail inhibitor concentration (FIC) of the scale inhibitor. This is not the same as the operational field use of the abbreviation MIC, which is the minimum inhibitor concentration that prevents scale formation. The removal of scale between tests was carried out using a 10 min injection of an aqueous solution of Na_2EDTA and NaOH having pH 12−13. This was followed by 10 min with deionized water.

https://doi.org/10.1021/acssuschemeng.1c06786
ACS Sustainable Chem. Eng. 2021, 9, 16494−16505

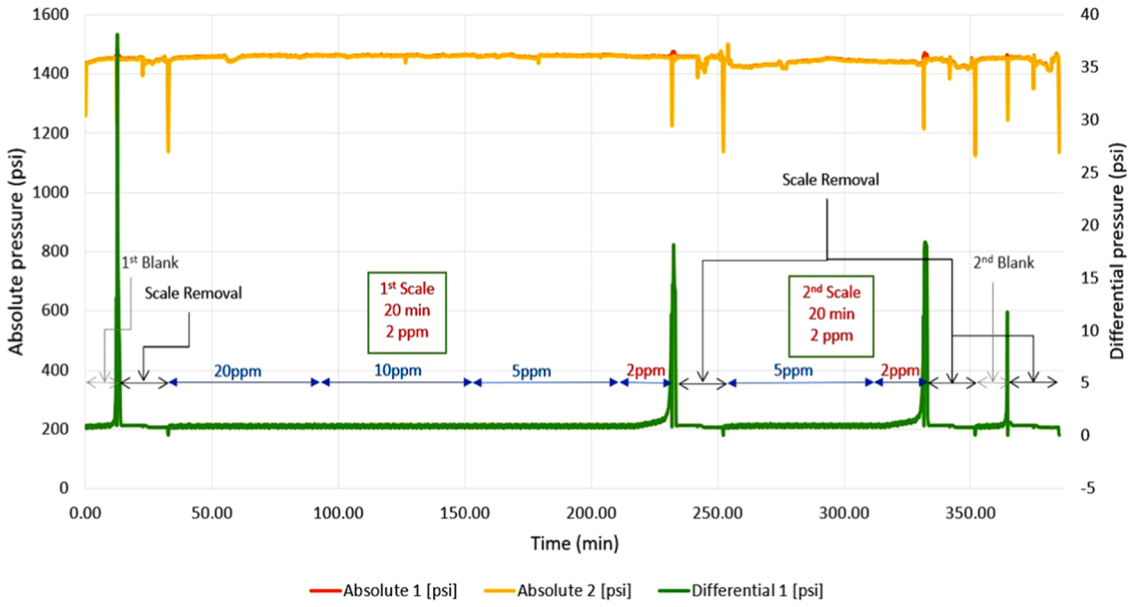

Figure 4. Graph showing the determination of blank and MIC scaling times.

Four tests are carried out in one run of the dynamic tube blocking rig. These are a blank test (no SI), the first SI test, a repeat SI test, and finally a second blank test. Figure 4 shows a typical graph obtained from a single run.

The produced water used in this investigation was based on the Heidrun field, which has seawater injection. (Table 1). The composition of the separate brines 1 and 2 for calcite and barite scaling are given in Tables 2 and 3, respectively. Brines were degassed for 15 min using a vacuum pump to remove dissolved gas that might cause the pump to stop brine injection due to gas bubbles in the line. Sodium bicarbonate was added to brine 2 after degassing to avoid disturbing the equilibrium between bicarbonate and dissolved CO_2.

In the example in Figure 4, we injected the SI at 20, 10, 5, and 2 ppm for 1 h each. After 20 min at 2 ppm, rapid scale formation occurred. After cleaning the coil, the repeat scale inhibitor test was carried out but starting from 5 ppm. After 20 min at 2 ppm, the scale formed rapidly again. This shows that the reproducibility of the experiments is very good, which was true for all experiments in this study. The final stage of the experiment was a new blank test without the addition of the inhibitor. We observed that the time for scaling in the second blank test is often a little longer than the first blank test, both for carbonate and sulfate scaling. This may be due to the time needed to flush out the distilled water cleaning fluid in the system, which is not present in the first blank test. Before the first blank test, we flushed the scaling brines, one at a time, to check for good flow in the system.

Table 1. Composition of Heidrun Formation Water, Seawater, and a 50/50 Mixture

ion	Heidrun formation water (ppm)	seawater (ppm)	50/50 mixed brine (ppm)
Na^+	19 510	10 890	15 200
Ca^{2+}	1020	428	724
Mg^{2+}	265	1368	816.5
K^+	545	460	502.5
Ba^{2+}	285	0	142.5
Sr^{2+}	145	0	72.5
SO_4^{2-}	0	2960	1480
HCO_3^-	880	120	500

Table 2. Salts Used to Make Brines 1 and 2 for Calcite Scaling

ion	ppm	component	brine 1 (g/5 L)	brine 2 (g/5 L)
Na^+	39 020	NaCl	247.97	247.97
Ca^{2+}	2040	$CaCl_2{\cdot}2H_2O$	37.42	
Mg^{2+}	530	$MgCl_2{\cdot}6H_2O$	22.16	
K^+	1090	KCl	10.39	
Ba^{2+}	570	$BaCl_2{\cdot}2H_2O$	5.07	
Sr^{2+}	290	$SrCl_2{\cdot}6H_2O$	4.41	
HCO_3^-	1000	$NaHCO_3$	0	13.76

Table 3. Salts Used to Make Brines 1 and 2 for Barite Scaling

ion	ppm	component	brine 1 (g/5 L)	brine 2 (g/5 L)
Na^+	15 200	NaCl	193.19	175.18
Ca^{2+}	724	$CaCl_2{\cdot}2H_2O$	26.56	
Mg^{2+}	807	$MgCl_2{\cdot}6H_2O$	68.28	
K^+	502	KCl	9.58	
Ba^{2+}	142.5	$BaCl_2{\cdot}2H_2O$	2.53	
Sr^{2+}	72.5	$SrCl_2{\cdot}6H_2O$	2.21	
SO_4^{2-}	1480	Na_2SO_4 anhydrous	0	21.88

Thermal Stability Test. Thermal aging is required to determine the scale inhibitor stability (ability to maintain performance) at high temperatures, particularly for a long squeeze lifetime.[34] A 5% W/V solution of the scale inhibitor in deionized water was prepared. The pH was adjusted to 4.5 (a typical downhole oilfield pH) using either aqueous NaOH or aqueous HCl, depending on the original pH. The solution was placed in a pressure tube, and air was replaced with a nitrogen atmosphere (anaerobic). The scale inhibitor solution was aged at 130 °C for 7 days. The solution was then retested for calcite and barite scale inhibition.

Compatibility Test. Different aqueous concentrations of calcium salt and scale inhibitors were mixed to check whether Ca^{2+}–SI complexation and deposition would occur. Calcium compatibility testing was carried out as follows: 20 mL of four concentrations of the scale inhibitor (100, 1000, 10 000, and 50 000 ppm) were prepared with four different concentrations of Ca^{2+} ions (10, 100, 1000, and 10 000 ppm) in synthetic seawater (3.00% NaCl). The pH of the mixture solution was adjusted to 4.0–4.5. The jars were shaken well,

https://doi.org/10.1021/acssuschemeng.1c06786
ACS Sustainable Chem. Eng. 2021, 9, 16494–16505

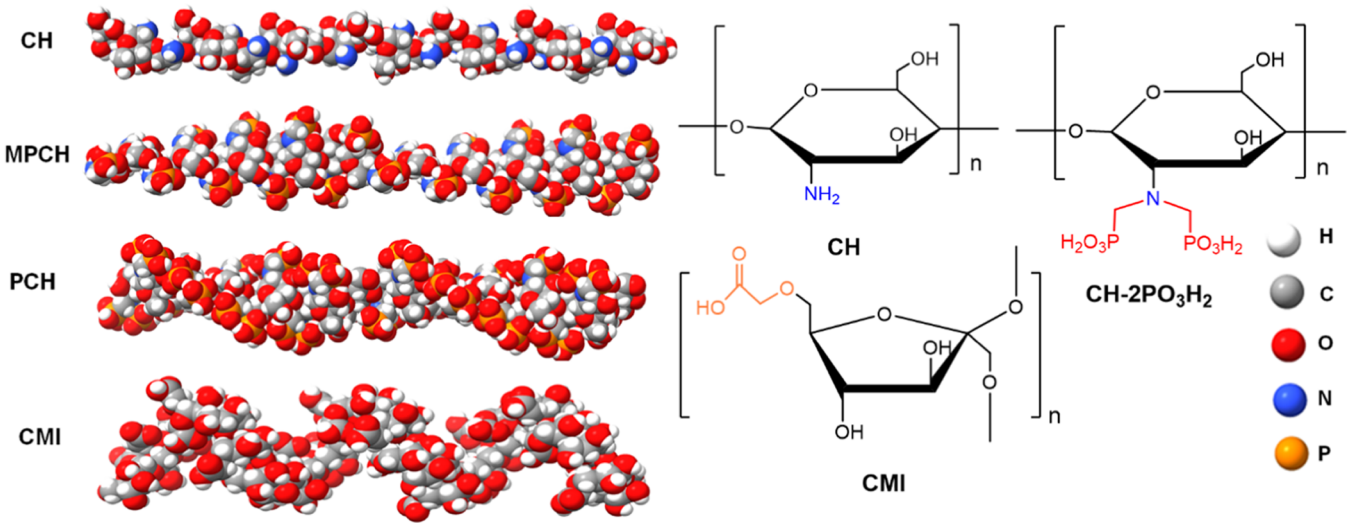

Figure 5. Minimized structures of the polysaccharide polymers (left) and their chemical structures (right) considered in our study. Chitosan (**CH**), monophosphonated chitosan (**MPCH**), bisphosphonated chitosan (**PCH**), and carboxymethyl inulin (**CMI**).

and the appearance of the mixture was checked at room temperature. All jars were then placed in an oven at 80 °C, and the appearance of the solution was inspected after 30 min, 1, 4, and 24 h, looking for any cloudiness and/or deposition. This method was repeated for all synthesized SIs to check for reproducibility.

Quantum Chemical Calculations. *DFT Periodic Model Simulations.* DFT simulations were carried out using the Vienna Ab initio Simulation Package (VASP)[35,36] with the projector augmented wave (PAW) pseudopotentials[37] and the periodic boundary conditions. The Brillouin zone was sampled using 3 × 3 ×1 Monkhorst-pack γ centered mesh,[38] and a Gaussian smearing of 0.02 eV was used for the occupations of the electronic levels. The Perdew–Burke–Ernzerhof (PBE)[39] functional within the generalized gradient approximation (GGA) was used to describe the electron interaction energy of exchange–correlation. The electronic energies were converged within the limit of 10^{-7} eV, and a cutoff of 520 eV was used. All geometries were optimized using 0.03 eV/Å force criteria. van der Waals (VDW) dispersion corrections are adopted using Grimme's D3 scheme.[40] The SI adsorption energies E_{ads} were calculated based on eq 1

$$E_{ads} = E_{Slab+SI} - [E_{Slab} + E_{SI}] \quad (1)$$

A 3 × 4 x 1 supercell for the 104 calcite facet[41] and a 2 × 4 × 1 supercell for the 001 barite facet were used. These are reported as the most stable facets of the calcite and barite crystals, respectively.[42] A vacuum of 15 Å was applied along the *Z*-axis to remove the spurious interaction that could occur between the surface and its image due to the periodic boundary condition. The thickness of the slab along the *Z*-axis is three layers, consisting of 240 atoms of calcite and 288 atoms of barite. Two layers are fixed during the geometry optimization, and the top third layer is allowed to relax.

Extended Tight-Binding Molecular Dynamics Simulations. Molecular dynamics (MD) simulations are performed on oligomers of 20-mer lengths to examine the polymer conformational changes that probably would impact their adsorption on the calcite and barite facets. The GFN2-xTB method[43] with the extended tight-binding Hamiltonian[44,45] was used to sample the polymer chain conformation due to its efficiency and including the electronic effects at the semiempirical level of theory, which are challenging systems for the DFT method.[39] The empirical FF parameters for the GFN2-xTB method are fitted to reproduce the results of DFT (B97-3c).[46] Figure 5 depicts two- and three-dimensional structures of the considered polymers in our MD simulations. Prior to MD production, an energy minimization step is performed to remove the bad atomic contacts in the initial polymer coordinates. All MD simulations were carried out at 300 K using the XTB code.[47]

RESULTS AND DISCUSSION

Synthesis of Phosphonated Chitosan (PCH). **PCH** is the bis-methylenephosphonate derivative of the amine functional groups of chitosan. **PCH** was synthesized via the Moedritzi–Irani reaction, which is a standard synthetic method used to make a range of oilfield aminophosphonate scale inhibitors.[23,24] This reaction is carried out at low pH and an elevated temperature using phosphorous acid, hydrochloric acid, and methanal (formaldehyde). A report suggests that it is a difficult method to carry out with hydrochloric acid on chitosan and is only possible if it is carried out with a large excess of phosphorous acid and formaldehyde added simultaneously and heated at 70 °C for many hours.[48]

Heras et al. used a 2% (w/v) chitosan solution in glacial acetic acid with phosphorous acid and methanal. They obtained both the mono- and disubstituted methylenephosphonates, together with some acetylation still present from the incomplete chitin hydrolysis.[22] We initially attempted to synthesize **PCH** in the first step using the Moedritzer–Irani reaction and the reaction conditions of Heras et al.[49] Chitosan was reacted with H_3PO_3 and HCHO in the presence of an aqueous acetic acid solution, as shown in Figure 2 (route A). ^{1}H and ^{31}P NMR were utilized to monitor and confirm the target compound. The ^{1}H NMR spectra of the sample reaction did not display a doublet peak related to C**H**$_2$-PO_3H_2. In addition, in the ^{31}P NMR spectra, we did not observe a significant signal corresponding to the PO_3H_2 group. In conclusion, we could not manage to synthesize **PCH** by the method reported by Heras et al.

Therefore, we decided to utilize the Kabachnik–Fields pathway (two-step synthesis route) to prepare **PCH** (Figure 2, route B). First, **CH** was reacted with dimethyl phosphite ($(CH_3O)P_2(O)H$) and methanal in the presence of an aqueous acetic acid solution at 70 °C to afford **CH–$PO_3(CH_3)_2$**. The ^{31}P NMR chemical shift of **CH–$PO_3(CH_3)_2$** revealed a singlet peak at δ 28.87. In the second step, the phosphonated diester chitosan was hydrolyzed using 1 M HCl to afford **CH–PO_3H_2**. It was found that the ^{1}H NMR displayed a distinct doublet peak at δ 3.51–3.54 ppm corresponding to –C**H**$_2$–PO_3H_2–, as illustrated in Figure 6b. Furthermore, the ^{31}P NMR chemical shift of **PCH** gave a

https://doi.org/10.1021/acssuschemeng.1c06786
ACS Sustainable Chem. Eng. 2021, 9, 16494–16505

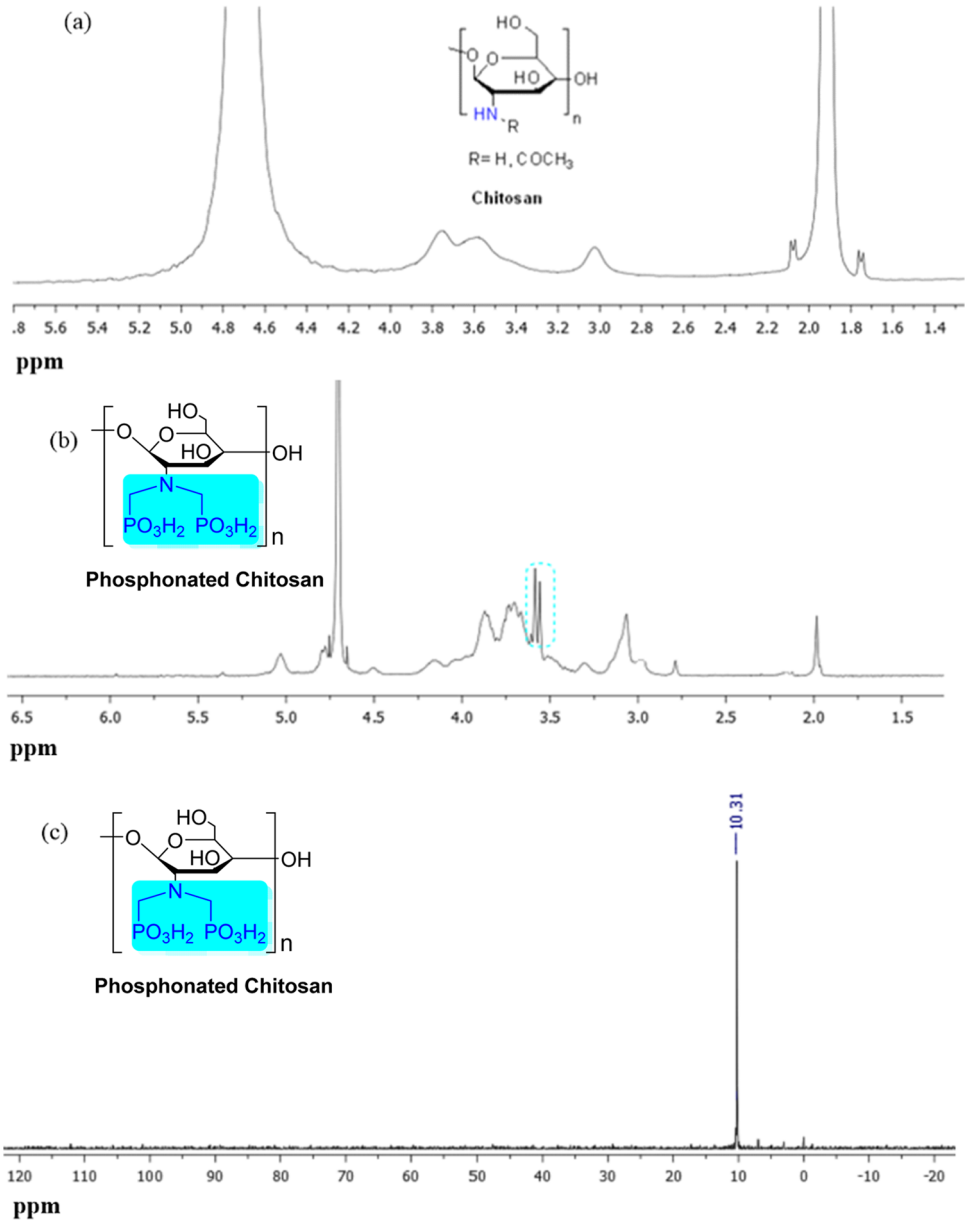

Figure 6. Schematic representation of the ^{1}H NMR spectra of chitosan (a) and phosphonated chitosan (b) and the ^{31}P NMR spectrum of phosphonated chitosan (c).

significant singlet signal at δ 10.31 ppm attributed to the phosphonic acid group (Figure 6c). We can conclude that the modified chitosan-bearing phosphonic acid group was successfully synthesized, and our findings matched well with the reported results of Illy et al. and others.[25,50,51]

High-Pressure Dynamic Tube Blocking Test. The results of scale inhibition tube blocking tests for calcite scale are summarized in Table 4. The performances of some common scale inhibitors, **ATMP**, **DTPMP**, and more biodegradable **CMI**, are included for comparison. The results show that **PCH** gave an FIC of 10 ppm after 31 and 32 min (Figure 7). This was comparable to the pentaphosphonate **DTPMP** and better than the triphosphonate **ATMP**. The polycarboxylate **CMI** performed better than **PCH** with an FIC of 5 ppm after 28 and 30 min.

Interestingly, after thermal aging of **PCH** for 1 week at 130 °C, there was no loss of calcite inhibition performance. In fact, the delay time at 10 ppm increased a little to 40 and 42 min

Table 4. Tube Blocking Results for Calcite Scale, Giving FIC Values for Commercial SIs and PCH before and after Thermal Aging

	calcite scale					
	1st blank	1st inhibitor test		2nd inhibitor test		2nd blank
scale inhibitor	time (min)	conc. (ppm)	time (min)	conc. (ppm)	time (min)	time (min)
ATMP	11	20	26	20	26	12
DTPMP	10	10	20	10	20	12
CMI	9	5	30	5	28	9
PCH	9	10	31	10	32	10
PCH[a]	10	10	40	10	42	11

[a]PCH was tested against calcite scale after thermal aging at 130 °C for 1 week.

https://doi.org/10.1021/acssuschemeng.1c06786
ACS Sustainable Chem. Eng. 2021, 9, 16494−16505

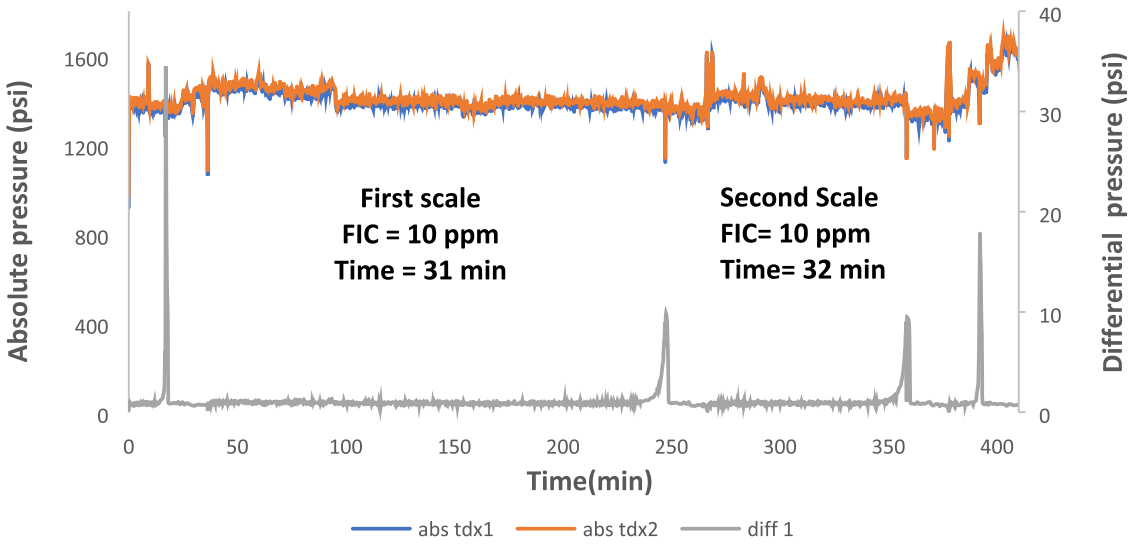

Figure 7. Schematic representation of the calcite scale dynamic scale loop test for **PCH**, showing FIC values and scaling times.

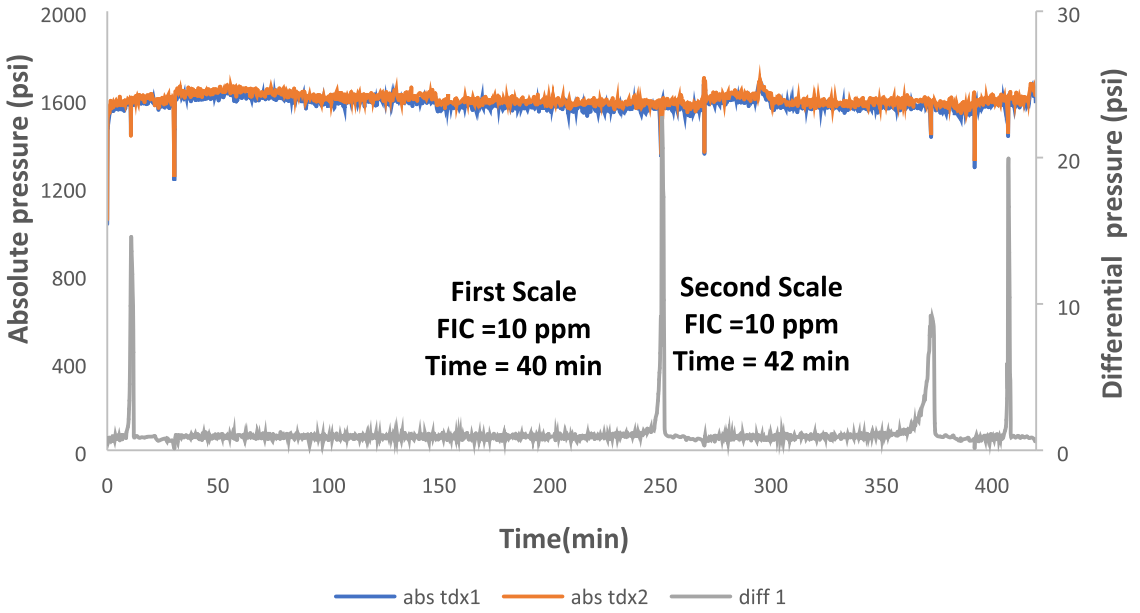

Figure 8. Schematic representation of the calcite scale dynamic scale loop test (FIC vs time) for **PCH** after thermal aging at 130 °C.

(Figure 8). We speculate that there might be some minor decomposition of the chitosan backbone to form shorter polymer chains. This would give more chains, each with several phosphonate groups. Bearing in mind that the chitosan used was the lowest molecular weight available (50 000−190 000 Da), it is quite possible that even shorter chitosan chains might give improved scale inhibition performance while still keeping the natural biodegradable polysaccharide backbone. However, shorter chitosan chains were not commercially available. In addition, we aged **CMI** at 130 °C for 1 week under anaerobic conditions. We found that the solution's color changed to black when the temperature was increased to 100 °C. So, we decided not to carry out dynamic scale inhibition tests on the thermally aged **CMI**.

The results of scale inhibition tube blocking tests for barite scale are summarized in Table 5. The performances of some common scale inhibitors, **ATMP**, **DTPMP**, and more biodegradable **CMI**, are included for comparison. In contrast to calcite inhibition, **PCH** was much worse as a barite scale inhibitor, worse than the commercial inhibitors. There was also no significant change in the performance of the thermally aged

Table 5. Tube Blocking Results for Barite Scale, Giving FIC Values for Commercial SIs and PCH before and after Thermal Aging

	barite scale					
	1st blank	1st inhibitor test		2nd inhibitor test		2nd blank
scale inhibitor	time (min)	conc. (ppm)	time (min)	conc. (ppm)	time (min)	time (min)
ATMP	11	10	42	10	41	11
DTPMP	10	5	5	5	9	10
CMI	10	5	12	5	12	11
PCH	11	100	21	100	20	10
PCH[a]	11	100	16	100	14	12

[a]PCH was tested against barite scale after thermal aging at 130 °C for 1 week.

https://doi.org/10.1021/acssuschemeng.1c06786
ACS Sustainable Chem. Eng. 2021, 9, 16494−16505

PCH sample (130 °C). This shows that the presence of a lot of phosphonate groups in the polymer is not critical for good barite inhibition. More important is the spacing of these groups.

Calcium Compatibility Test. Oilfield formation water often contains a high amount of calcium ions. Seawater also contains about 400 ppm of these ions. Some scale inhibitors, particularly phosphonates are not very compatible with calcium ions, forming insoluble SI−Ca complexes. Inhibitors must be tolerant of any water they will meet after injection to avoid SI−Ca complex precipitation. If the inhibitor is used for squeeze treatments, it could cause formation damage. The results of the calcium compatibility test for **PCH** are given in Table 6. As the table shows, **PCH** was fully compatible at all concentrations, even with 50 000 ppm (5 wt %) inhibitor concentration and 10 000 ppm Ca^{2+} ions compared to the conventional SI **DTPMP**. It was found that **DTPMP** was not compatible at all tested SI concentrations (1000−50 000 ppm) and 1000 ppm Ca^{2+} ions, as shown in the Supporting Information.

Table 6. Compatibility Test in 10 000 ppm Ca^{2+} and 30 000 ppm (3.0 wt %) NaCl for PCH

	appearance				
dose (ppm)	at mixing	30 min	1 h	4 h	24 h
100	clear	clear	clear	clear	clear
1000	clear	clear	clear	clear	clear
10 000	clear	clear	clear	clear	clear
50 000	clear	clear	clear	clear	clear

A possible reason for the excellent compatibility is the hydroxyl and ether groups in the polysaccharide chain. Ether linkages have previously been shown to improve the calcium compatibility of aminophosphonates.[27]

Quantum Chemical Studies. *Polymer Adsorption on the Mineral Surfaces.* Solid-state DFT simulations are carried out to gain atomic insights into the adsorption of the considered polymers on the most stable facets of the calcite and barite minerals. In this study, we have studied the adsorption of one repeating unit of each polymer on the 104 facet of calcite and the 001 facet of barite. We have considered the adsorption of **ATMP** as a reference case. The results reported in Table 7 indicate that the considered repeating units display good affinities for both minerals. The phosphonated chitosan displays very favorable interaction with both calcite and barite surfaces and is close to **ATMP** interaction energies. However, it exhibits stronger binding to the calcite facet than the barite facet, which is in agreement with our experimental results. We found that the bisphosphonated chitosan (**PCH**) binds more tightly to the mineral surfaces than the monophosphonated chitosan (**MPCH**). The **Ca−O_3P** bond distances in the case of the calcite−**PCH** complex are shorter than **Ba−O_3P** bonds in the barite−**PCH** complex (Figure 9). This is applied for all of the adsorbed chemical structures considered in our study, the interaction distances are shorter for calcite than for barite. Further, all of the examined building units display better adsorption energies on calcite than on barite, which is basically due to the surface morphologies and the ionic charge densities of Ca^{2+} and Ba^{2+}. The ionic size difference between Ca^{2+} and Ba^{2+} ions makes the charge densities on Ca^{2+} higher and therefore stronger interactions with SIs. In addition, the tetrahedral geometry of the $[SO_4]^{2-}$ group makes it more surface exposed than linear $[CO_3]^{2-}$, which leads to more electrostatic repulsion on the barite surface than on calcite. Concerning the interaction of **MPCH** with the mineral facets, we found that the binuclear mode of interaction (Figures 9 and S1) is stronger than the mononuclear mode of interaction (Figure S1).

Table 7. Adsorption Energies of the Considered SI Inhibitors on Calcite 104 and Barite 001 Facets (Reported in eV)[a]

SIs	calcite	barite
PCH	−13.3	−12.40
MPCH	−5.3 (−3.9)	−4.3 (−2.7)
CH	−1.45	−0.97
CMI	−1.30	−0.92
ATMP	−16.0	−16.2

[a]In parenthesis, the adsorption energies of **MPCH** adsorbed in the mononuclear mode are reported (Figure S1).

The polycarboxylate **CMI** polymer shows a good adsorption affinity on both calcite and barite with more preference to the calcite surface. However, the **CH** unit is exhibiting adsorption affinities higher than the **CMI** unit (Table 7), while the **CMI** polymer is experimentally outperforming the **CH** polymer. The modeling study shows that the mode of interaction of both units is completely different. The molecular axis of the **CH** unit is parallel to the mineral facet, while the **CMI** unit displays a mononuclear mode of interaction via its carboxylate. The interaction of the **CH** unit on both minerals takes place through hydrogen bonds (NH_2 and OH groups) and van der Waals (VDW) forces. **CMI** adsorbs on the mineral surfaces mainly by electrostatic interactions between the metal cation and its carboxylate. Such **CH** mode of interaction on the mineral facet is not possible due to the polymer conformational restraints, while the **CMI** polymer still possesses dangling carboxylate groups that can interact with the mineral surface (see the section GFN2-xTB Molecular Dynamics Simulations).

The adsorption energies reported in Table 7 predict that the individual building units of **CH**, **PCH**, **MPCH**, and **CMI** should be good scale inhibitors. However, **FIC** data reported in Tables 4 and 5 show that **CMI** is better than **PCH** and even better than **ATMP** for both calcite and barite scale inhibition. These results raise an important question about the mechanism by which the polymeric materials inhibit the calcite and barite scales. It is evident that the direct interaction of the repeating unit of the polymeric materials with the mineral surfaces is not enough to fully explain the inhibition mechanism. In our DFT simulation, we found that **ATMP** is binding better than the repeating units of all of the considered polymers, while **CMI** performed better than **ATMP**.

Further, **ATMP** performs better for the calcite scale than the barite scale, though it interacts almost similarly with the two facets as DFT predicted. Therefore, we hypothesize that the polymer conformation might play an important role in the inhibition mechanism. To check the validity of our hypothesis, we have performed molecular dynamics simulations using the extended tight-binding (xTB) semiempirical quantum method with its variant GFN2-xTB method.

GFN2-xTB Molecular Dynamics Simulations. GF2-xTB MD simulations are carried out on **CH**, **MPCH**, **PCH**, and **CMI** polymers to gain insights into their chain morphologies in

https://doi.org/10.1021/acssuschemeng.1c06786
ACS Sustainable Chem. Eng. 2021, 9, 16494−16505

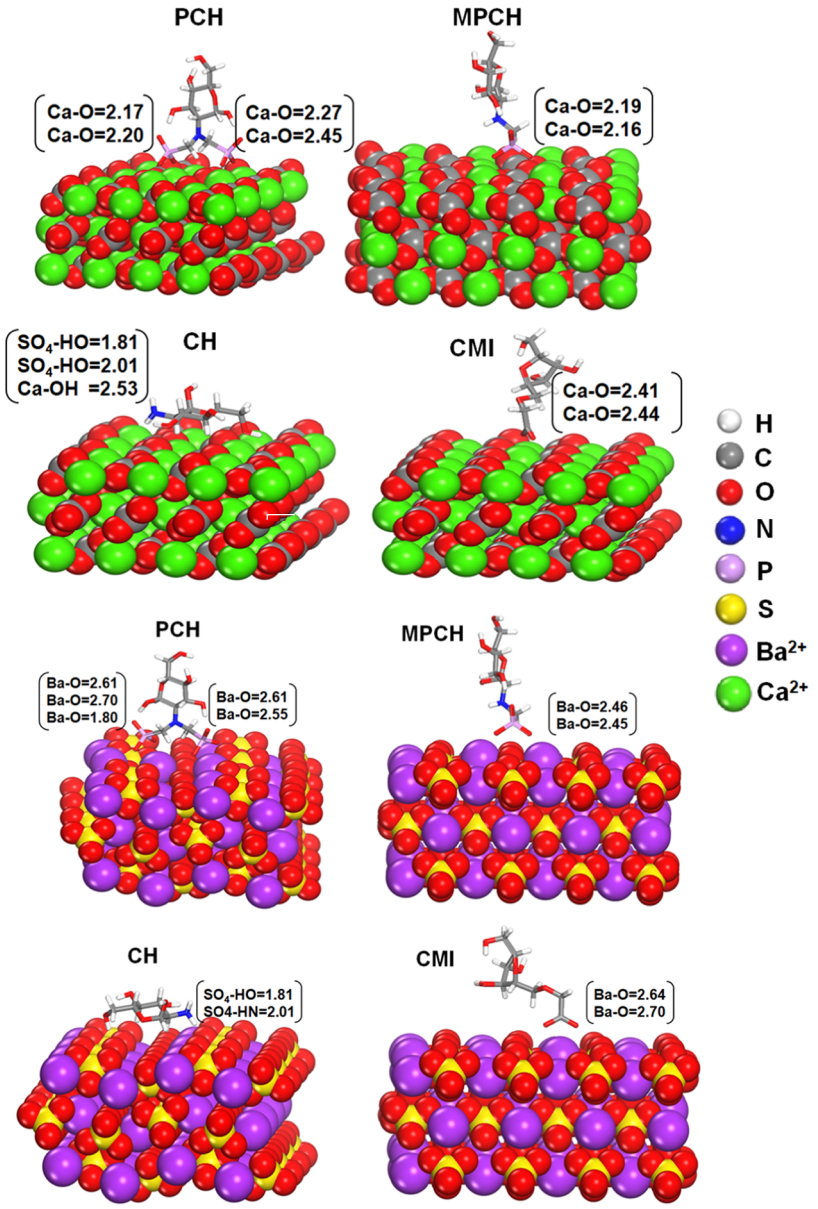

Figure 9. Optimized structures of one repeating unit of the considered polymers in our DFT simulations on the calcite (104) and barite (001) facets. The bond distance of metal−oxygen and the hydrogen bonds are reported in Å. The atomic color code is shown.

an implicit water phase. **CH** was found to be very stable and exhibits a rigid backbone in an extended conformation (Figures 10 an 11d). The **PCH** polymers are curled up in more compact conformations due to the high degree of internal hydrogen bond networks (Figures 10 and 11). **CMI** wraps into a helical structure, and it is quite stable during the whole trajectory. It is true that the **CMI** polymer is folded into more compact conformations compared to the initial extended structure (Figures 5, 10, and 11). However, it is still not as compact as **PCH**. The radius of gyration (**Rg**) of **CMI** changes from 17.0 to 11.0 Å, while those of **MPCH** and **PCH** change from 23.4 to 9.5 and 23.4 to 12.0 Å, respectively. The conformational contraction of **PCH** polymers is more significant than that of the **CMI** polymer. Indeed, **MPCH** is contracted by 60% of its initial volume and **PCH** by 48%, while **CMI** loses 35% of its initial volume. The same trend is observed for the end-to-end distances (Figure 11).

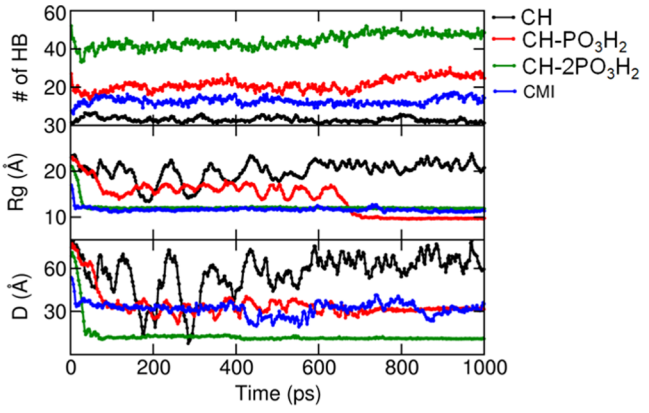

Figure 10. Internal hydrogen bonds of the four considered polymers, their radius of gyration, and end-to-end distances are shown as a function of simulation time.

https://doi.org/10.1021/acssuschemeng.1c06786
ACS Sustainable Chem. Eng. 2021, 9, 16494−16505

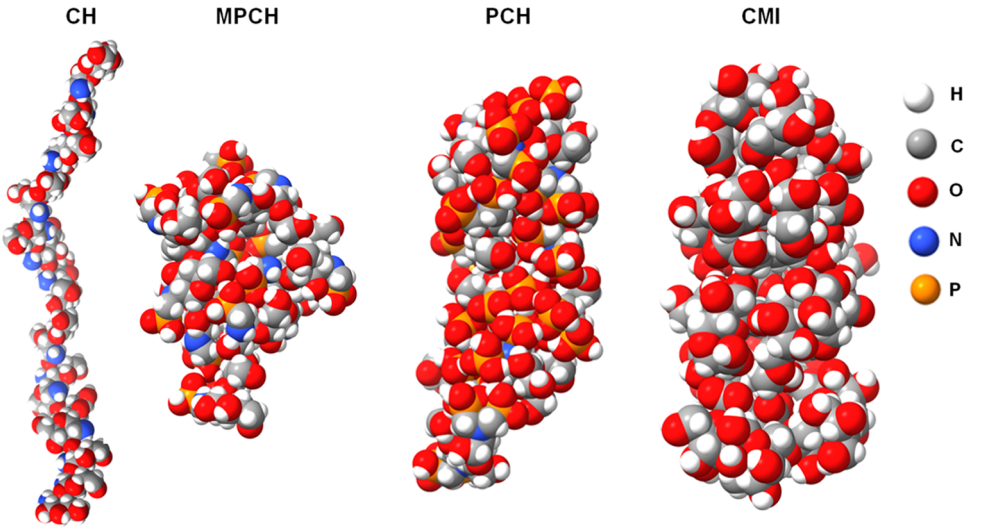

Figure 11. Sphere representations of 1 ns snapshots of polymer chains showing the final morphology of the four polymers. Color code; O: red, H: white, N: blue, C: olive, and P: orange.

The significant conformational contraction of **PCH** could be the cause of its lower performance compared to the **CMI** polymer for the calcite inhibition. DFT and GFN2-xTB MD simulations reveal that a complicated scale inhibition mechanism takes place when we apply polymeric materials. The conformational changes of the polymer chain play an important role. These conformational states display different modes of interactions with the small mineral particles, which serve as nucleation sites for the growth of the scales.

It is true that the polymer adopts different conformations and even more compact structures. However, they still display adsorption sites (the phosphonate and carboxylate groups) on which the calcite or barite particles can be docked. The induced-fit process of the polymer structures, to maximize the geometric matching between the mineral surfaces and the polymer, should be an important step along the inhibition pathway. The conformational diversity of the polymeric materials makes such a process complicated to figure out using only the DFT results of the direct interaction. For the barite scale, the kinetics is sluggish and complicated; it involves amorphous and crystalline aggregates.[52] The final crystalline particles are obtained through the restructuring of the amorphous aggregates, which is a slow kinetic process. Thus, the inhibition of the barite scale requires the application of a higher concentration of polymeric materials.

Altogether, DFT and GFN2-xTB MD simulations bring new insights into the inhibition mechanism of polymeric materials. DFT predicted the importance of the mode of adsorption on the mineral−SI recognition thermodynamics. MD simulations predicted that the conformational contraction of the polymeric materials could affect the polymer performance (**PCH** vs **CMI**). Using a combination of DFT and MD simulations, we could explain the performance of **CMI** compared to **ATMP**. Small molecules (**ATMP**) dock on the mineral surface, while polymeric materials (**CMI** and **PCH**) serve as docking sites of the mineral particles. In this scenario, more mineral particles can be absorbed on the polymer surface than the small molecules. The strong direct interactions are not decisive to define the final stable mineral−SI complex. Yet, the morphology of SIs (polymers) is an important parameter to determine the thermodynamic stability of the mineral−SI complex. Consequently, the distribution of the functional groups (carboxylate and phosphonates) on the polymer surface is very important for optimal performance. Indeed, carboxylate groups are distributed on the **CMI** polymer surface in a regular pattern due to its well-defined and stable helical structure. **PCH** exhibits random and compact structures, which impact the availability of functional groups (phosphonates) to interact with the mineral surface compared to **CMI**. Further, the brine salinity (i.e., the free cations Na^+, Mg^{2+}, and Ca^{2+}) could interact with the polymer functional groups (phosphonate and carboxylate) and interfere with the mineral−SI interaction and affect the inhibition thermodynamics. For example, phosphonate groups interact more with the divalent cations than carboxylate groups.[26]

CONCLUSIONS

The synthesis of phosphonated chitosan (**PCH**) via the Moedritzi−Irani reaction failed in our hands. Therefore, it was prepared by a two-step route via the phosphonate ester. **PCH** showed excellent calcium compatibility up to 10 000 ppm Ca^{2+} and 50 000 ppm **PCH** for 24 h at 80 °C.

In dynamic tube blocking tests, **PCH** showed good performance as a calcium carbonate scale inhibitor, similar to the commercial nonpolymeric aminophosphonates **DTPMP**. Performance was not lost even after thermal aging as a 5 wt % aqueous anaerobic solution for 1 week at 130 °C. The performance as a barite inhibitor was shown to be significantly worse. Given the fact that SIs adsorbed on rocks are more stable than in solution, the data suggest that **PCH** could be a candidate for SI squeeze treatments for calcite scaling in wells where the downhole temperature is up to 130 °C.[10] DFT simulations predicted that the **PCH** polymer displays highly favorable interactions with both mineral surfaces (calcite and barite). DFT also reveals a complicated inhibition mechanism in the case of polymeric materials compared to small molecules. The direct interaction energies predicted by DFT could not fully explain **PCH** performance. Using MD simulations, we found that **PCH** undergoes a significant conformational contraction due to an intense hydrogen bonding network. The final polymer morphology has a random compact structure with exposed phosphonate groups

https://doi.org/10.1021/acssuschemeng.1c06786
ACS Sustainable Chem. Eng. 2021, 9, 16494−16505

serving as docking sites for the small mineral particles. The conformational diversity of the polymer morphology makes the mechanism very complex, and it is difficult to fully understand. The high density of the interaction sites on the **PCH** surface could be the origin of its higher performance compared to **ATMP**. The distribution of the functional groups on the polymeric material is found to be critical for scale inhibition. The **CMI** polymer exhibits a stable and well-defined helical structure with regular distribution of the functional groups (carboxylate) able to inhibit both scales efficiently. However, **PCH** is folded into random compact structures, which minimize the interaction sites with the mineral surfaces compared to **CMI**.

Furthermore, the sluggish kinetics of the barite crystal could explain the bad performance of **PCH** for the barite scale. The barite crystal displays multiple thermodynamics states along its formation pathway. It starts with amorphous particles that undergo restructuring into crystalline ones, which increase the possibilities of interaction with **PCH** and hence require high polymer concentrations to be inhibited.

■ ASSOCIATED CONTENT

Supporting Information

The Supporting Information is available free of charge at https://pubs.acs.org/doi/10.1021/acssuschemeng.1c06786.

> Figure of the optimized structures of the repeating unit of CH−PO_3 on the facets of calcite (104) and barite (001) with the mononuclear mode of interaction; figure of the dynamic tube blocking rig, and tolerance tests in 1000 ppm Ca^{+2} and 30 000 ppm (3.0 wt %) NaCl for **DTPMP** (Table S1) (PDF)

■ AUTHOR INFORMATION

Corresponding Author

Mohamed F. Mady − *Department of Chemistry, Bioscience and Environmental Engineering, Faculty of Science and Technology, University of Stavanger, N-4036 Stavanger, Norway; Department of Green Chemistry, National Research Centre, Cairo 12622, Egypt;* orcid.org/0000-0002-4636-0066; Email: mohamed.mady@uis.no

Authors

Safwat Abdel-Azeim − *Center of Integrative Petroleum Research, College of Petroleum and Geosciences, King Fahd University of Petroleum and Minerals, Dhahran 31261, Saudi Arabia;* orcid.org/0000-0001-8611-1251

Malcolm A. Kelland − *Department of Chemistry, Bioscience and Environmental Engineering, Faculty of Science and Technology, University of Stavanger, N-4036 Stavanger, Norway;* orcid.org/0000-0003-2295-5804

Complete contact information is available at: https://pubs.acs.org/10.1021/acssuschemeng.1c06786

Notes

The authors declare no competing financial interest.

■ ACKNOWLEDGMENTS

S.A.-A. thanks the Supercomputer Shaheen at King Abdullah University of Science & Technology (KAUST) in Thuwal, Saudi Arabia, for using its computational resources.

■ ABBREVIATIONS

CH, chitosan
PCH, phosphonated chitosan
MPCH, monophosphonated chitosan
CMI, carboxymethyl inulin
ATMP, aminotrismethylenephosphonic acid
DTPMP, diethylenetriaminepentamethylenephosphonic acid
HPHT, high-pressure high-temperature
CMCH, carboxymethylchitosan
CH−$PO_3(CH_3)_2$, phosphonated diester chitosan

■ REFERENCES

(1) Kelland, M. A. *Production Chemicals for the Oil and Gas Industry*; CRC press: Boca Raton, 2014.
(2) Frenier, W. W.; Ziauddin, M. *Formation, Removal, and Inhibition of Inorganic Scale in the Oilfield Environment*; Society of Petroleum Engineers Richardson: TX, 2008.
(3) Amjad, Z. *The Science and Technology of Industrial Water Treatment*; CRC press: Boca Raton, 2010.
(4) Amjad, Z.; Demadis, K. D. *Mineral Scales and Deposits: Scientific and Technological Approaches*; Elsevier: Amsterdam, 2015.
(5) Zhang, H.; Luo, X.; Lin, X.; Tang, P.; Lu, X.; Yang, M.; Tang, Y. Biodegradable Carboxymethyl Inulin as a Scale Inhibitor for Calcite Crystal Growth: Molecular Level Understanding. *Desalination* **2016**, *381*, 1−7.
(6) Verraest, D. L.; Peters, J. A.; van Bekkum, H.; van Rosmalen, G. M. Carboxymethyl Inulin: A New Inhibitor for Calcium Carbonate Precipitation. *J. Am. Oil Chem. Soc.* **1996**, *73*, 55−62.
(7) Kohler, N.; Ropital, F.; Courbin, G.; Estievenart, C. In *Polyaspartates: BiodegradableAlternates to Polyacrylates or Noteworthy Multifunctional Inhibitors?*, CORROSION 2002; OnePetro: Denver, Colorado, Paper Number: NACE-02411, April 7−11, 2002.
(8) Quan, Z.; Chen, Y.; Wang, X.; Shi, C.; Liu, Y.; Ma, C. Experimental Study on Scale Inhibition Performance of a Green Scale Inhibitor Polyaspartic Acid. *Sci. China, Ser. B: Chem.* **2008**, *51*, 695−699.
(9) Kirboga, S.; Öner, M. Investigation of Calcium Carbonate Precipitation in the Presence of Carboxymethyl Inulin. *CrystEngComm* **2013**, *15*, 3678−3686.
(10) Chen, P.; Hagen, T.; MacLean, A.; Selle, O. M.; Stene, K.; Wat, R. In *Meeting the Challenges of Downhole Scale Inhibitor Selection for an Environmentally Sensitive Part of the Norwegian North Sea*, International Symposium on Oilfield Scale; OnePetro: Aberdeen, United Kingdom, 2002.
(11) Muzzarelli, R. A. *Chitin*; Pergamon Press: Oxford, 1977.
(12) Kou, S.; Peters, L.; Mucalo, M. Chitosan: A Review of Sources and Preparation Methods. *Int. J. Biol. Macromol.* **2021**, *169*, 85−94.
(13) Ravi Kumar, M. N. V. A Review of Chitin and Chitosan Applications. *React. Funct. Polym.* **2000**, *46*, 1−27.
(14) Macedo, R. G. M. deA.; Marques, N. doN.; Paulucci, L. C.; Cunha, J. V. M.; Villetti, M. A.; Castro, B. B.; Balaban, R. deC. Water-Soluble Carboxymethylchitosan as Green Scale Inhibitor in Oil Wells. *Carbohydr. Polym.* **2019**, *215*, 137−142.
(15) Zhang, H.; Cai, Z.; Jin, X.; Sun, D.; Wang, D.; Yang, T.; Zhang, J.; Han, X. Preparation of Modified Oligochitosan and Evaluation of Its Scale Inhibition and Fluorescence Properties. *J. Appl. Polym. Sci.* **2015**, *132*, No. 42518.
(16) Guo, X.; Qiu, F.; Dong, K.; Zhou, X.; Qi, J.; Zhou, Y.; Yang, D. Preparation, Characterization and Scale Performance of Scale Inhibitor Copolymer Modification with Chitosan. *J. Ind. Eng. Chem.* **2012**, *18*, 2177−2183.
(17) Jones, F.; Oliveira, A.; Rohl, A. L.; Parkinson, G. M.; Ogden, M. I.; Reyhani, M. M. Investigation into the Effect of Phosphonate Inhibitors on Barium Sulfate Precipitation. *J. Cryst. Growth* **2002**, *237*−*239*, 424−429.

(18) Spinthaki, A.; Stathoulopoulou, A.; Demadis, K. D. The Interplay between Cationic Polyethyleneimine and Anionic Polyelectrolytes for the Control of Silica Scale Formation in Process Waters. *Int. J. Corros. Scale Inhib.* **2015**, *4*, 125−138.
(19) Demadis, K. D.; Pachis, K.; Ketsetzi, A.; Stathoulopoulou, A. Bioinspired Control of Colloidal Silica in Vitro by Dual Polymeric Assemblies of Zwitterionic Phosphomethylated Chitosan and Polycations or Polyanions. *Adv. Colloid Interface Sci.* **2009**, *151*, 33−48.
(20) Demadis, K. D.; Ketsetzi, A.; Pachis, K.; Ramos, V. M. Inhibitory Effects of Multicomponent, Phosphonate-Grafted, Zwitterionic Chitosan Biomacromolecules on Silicic Acid Condensation. *Biomacromolecules* **2008**, *9*, 3288−3293.
(21) Demadis, K. D.; Preari, M.; Antonakaki, I. Naturally Derived and Synthetic Polymers as Biomimetic Enhancers of Silicic Acid Solubility in (Bio) Silicification Processes. *Pure Appl. Chem.* **2014**, *86*, 1663−1674.
(22) Heras, A.; Rodríguez, N. M.; Ramos, V. M.; Agulló, E. N-Methylene Phosphonic Chitosan: A Novel Soluble Derivative. *Carbohydr. Polym.* **2001**, *44*, 1−8.
(23) Ramos, V. M.; Rodrıguez, N. M.; Rodrıguez, M. S.; Heras, A.; Agullo, E. Modified Chitosan Carrying Phosphonic and Alkyl Groups. *Carbohydr. Polym.* **2003**, *51*, 425−429.
(24) Ramos, V. M.; Rodrıguez, N. M.; Dıaz, M. F.; Rodrıguez, M. S.; Heras, A.; Agullo, E. N-Methylene Phosphonic Chitosan. Effect of Preparation Methods on Its Properties. *Carbohydr. Polym.* **2003**, *52*, 39−46.
(25) Illy, N.; Couture, G.; Auvergne, R.; Caillol, S.; David, G.; Boutevin, B. New Prospects for the Synthesis of N-Alkyl Phosphonate/Phosphonic Acid-Bearing Oligo-Chitosan. *Rsc Adv.* **2014**, *4*, 24042−24052.
(26) Mady, M. F.; Abdel-Azeim, S.; Kelland, M. A. Antiscaling Evaluation and Quantum Chemical Studies of Nitrogen-Free Organophosphorus Compounds for Oilfield Scale Management. *Ind. Eng. Chem. Res.* **2021**, *60*, 12175−12188.
(27) Mady, M. F.; Bayat, P.; Kelland, M. A. Environmentally Friendly Phosphonated Polyetheramine Scale Inhibitors—Excellent Calcium Compatibility for Oilfield Applications. *Ind. Eng. Chem. Res.* **2020**, *59*, 9808−9818.
(28) Mady, M. F.; Rehman, A.; Kelland, M. A. Synthesis and Antiscaling Evaluation of Novel Hydroxybisphosphonates for Oilfield Applications. *ACS Omega* **2021**, *6*, 6488−6497.
(29) Mady, M. F.; Malmin, H.; Kelland, M. A. Sulfonated Nonpolymeric Aminophosphonate Scale Inhibitors—Improving the Compatibility and Biodegradability. *Energy Fuels* **2019**, *33*, 6197−6204.
(30) Mady, M. F.; Fevang, S.; Kelland, M. A. Study of Novel Aromatic Aminomethylenephosphonates as Oilfield Scale Inhibitors. *Energy Fuels* **2019**, *33*, 228−237.
(31) Mady, M. F.; Charoensumran, P.; Ajiro, H.; Kelland, M. A. Synthesis and Characterization of Modified Aliphatic Polycarbonates as Environmentally Friendly Oilfield Scale Inhibitors. *Energy Fuels* **2018**, *32*, 6746−6755.
(32) Mady, M. F.; Kelland, M. A. Study on Various Readily Available Proteins as New Green Scale Inhibitors for Oilfield Scale Control. *Energy Fuels* **2017**, *31*, 5940−5947.
(33) Mady, M. F.; Bagi, A.; Kelland, M. A. Synthesis and Evaluation of New Bisphosphonates as Inhibitors for Oilfield Carbonate and Sulfate Scale Control. *Energy Fuels* **2016**, *30*, 9329−9338.
(34) Mady, M. F.; Rehman, A.; Kelland, M. A. Synthesis and Study of Modified Polyaspartic Acid Coupled Phosphonate and Sulfonate Moieties As Green Oilfield Scale Inhibitors. *Ind. Eng. Chem. Res.* **2021**, *60*, 8331−8339.
(35) Kresse, G.; Hafner, J. Ab Initio Molecular Dynamics for Liquid Metals. *Phys. Rev. B* **1993**, *47*, 558−561.
(36) Kresse, G.; Hafner, J. Ab Initio Molecular-Dynamics Simulation of the Liquid-Metal−Amorphous-Semiconductor Transition in Germanium. *Phys. Rev. B* **1994**, *49*, 14251−14269.
(37) Blöchl, P. E. Projector Augmented-Wave Method. *Phys. Rev. B* **1994**, *50*, 17953−17979.
(38) Monkhorst, H. J.; Pack, J. D. Special Points for Brillouin-Zone Integrations. *Phys. Rev. B* **1976**, *13*, 5188−5192.
(39) Perdew, J. P.; Burke, K.; Ernzerhof, M. Generalized Gradient Approximation Made Simple. *Phys. Rev. Lett.* **1996**, *77*, 3865−3868.
(40) Grimme, S. Semiempirical GGA-Type Density Functional Constructed with a Long-Range Dispersion Correction. *J. Comput. Chem.* **2006**, *27*, 1787−1799.
(41) Bano, A. M.; Rodger, P. M.; Quigley, D. New Insight into the Stability of CaCO3 Surfaces and Nanoparticles via Molecular Simulation. *Langmuir* **2014**, *30*, 7513−7521.
(42) Jones, F.; Richmond, W. R.; Rohl, A. L. Molecular Modeling of Phosphonate Molecules onto Barium Sulfate Terraced Surfaces. *J. Phys. Chem. B* **2006**, *110*, 7414−7424.
(43) Bannwarth, C.; Ehlert, S.; Grimme, S. GFN2-XTB—An Accurate and Broadly Parametrized Self-Consistent Tight-Binding Quantum Chemical Method with Multipole Electrostatics and Density-Dependent Dispersion Contributions. *J. Chem. Theory Comput.* **2019**, *15*, 1652−1671.
(44) Bannwarth, C.; Caldeweyher, E.; Ehlert, S.; Hansen, A.; Pracht, P.; Seibert, J.; Spicher, S.; Grimme, S. Extended Tight-Binding Quantum Chemistry Methods. *WIREs Comput. Mol. Sci.* **2021**, *11*, No. e1493.
(45) Pracht, P.; Caldeweyher, E.; Ehlert, S.; Grimme, S. A Robust Non-Self-Consistent Tight-Binding Quantum Chemistry Method for Large Molecules. *ChemRxiv. Cambridge: Cambridge Open Engage* **2019**, 1−19.
(46) Brandenburg, J. G.; Bannwarth, C.; Hansen, A.; Grimme, S. B97-3c: A Revised Low-Cost Variant of the B97-D Density Functional Method. *J. Chem. Phys.* **2018**, *148*, No. 064104.
(47) *Semiempirical Extended Tight-Binding Program Package Xtb*. Version 6.4.1; https://github.com/grimme-lab/xtb, 2021.
(48) Lebouc, F.; Dez, I.; Madec, P.-J. NMR Study of the Phosphonomethylation Reaction on Chitosan. *Polymer* **2005**, *46*, 319−325.
(49) Moedritzer, K.; Irani, R. R. The Direct Synthesis of α-Aminomethylphosphonic Acids. Mannich-Type Reactions with Orthophosphorous Acid. *J. Org. Chem.* **1966**, *31*, 1603−1607.
(50) Lebouc, F.; Dez, I.; Gulea, M.; Madec, P.-J.; Jaffres, P.-A. Synthesis of Phosphorus-Containing Chitosan Derivatives. *Phosphorus, Sulfur Silicon Relat. Elem.* **2009**, *184*, 872−889.
(51) Kuhn, M. D.; Maier, T. D.; Stehlin, A. Phosphonomethylated Chitosans. EP0713882A1, May 29, 1996.
(52) Jones, F.; Piana, S.; Gale, J. D. Understanding the Kinetics of Barium Sulfate Precipitation from Water and Water−Methanol Solutions. *Cryst. Growth Des.* **2008**, *8*, 817−822.

https://doi.org/10.1021/acssuschemeng.1c06786
ACS Sustainable Chem. Eng. 2021, 9, 16494−16505